Effect of Clay Amounts on Morphology and Mechanical Performances in Multiscale PET Composites

C. N. Barbosa[1], F.Chabert*, V.Nassiet*, J. C. Viana[2], P. Pereira[3]

IPC/I3N – Institute for Polymers and Composites, Department of Polymer Engineering
University of Minho, 4800-058 Guimarães, Portugal
[1]cbnuno@dep.uminho.pt, [2]*jcv@dep.uminho.pt*, [3]*ppereira@dep.uminho.pt*
**Interfaces and Functional Materials, Production Engineering Research Laboratory,*
ENIT Ecole Nationale d'Ingénieurs de Tarbes， 65016 Tarbes, France

Abstract. This work presents an investigation of the properties of poly(ethylene terephthalate)/glass fibers/nanoclay multiscale composites. The aim is to demonstrate the effect of adding various clay amounts on the morphology and mechanical performances of multiscale PET composites. Multiscale composites were prepared by adding 0.5, 1.0, 3.0, and 5.0 wt% of Cloisite 15A montmorrillonite. Initially, a masterbatch of pure PET blended with 10 wt% of Cloisite 15A was obtained in a co-rotating twin screw extruder. The multiscale composites were then blended via mechanical mixing, and injection moulded by adding the masterbatch to the glass fibre reinforced matrix. The morphological and mechanical characterizations of all compounds are discussed. X-ray diffraction (XRD) and transmission electron microscopy (TEM) revealed that the characteristic (001) peak of the nanocomposite obtained by extrusion (masterbatch) shifted to the lower angle region stating an intercalated structure. However, the subsequent injection moulding process changed the morphological structure of the multiscale nanocomposites reducing the basal distance mostly for small loadings of nanoclay. The addition of nanoclay to PET matrices increases the degree of crystallinity, the clay platelets possibly playing the role of nucleating agent, as revealed by DSC and FTIR. The time relaxation spectra broaden as seen by DMA, as the ratio of clay/polymer interfaces increases. The yield stress of composites with 0.5 and 1 wt% of C15A content are enhanced. For more than 3% of nanoclay, the yield stress decreases. The Young's modulus is increased when adding nanoclay. Indeed, clay exfoliation was not attained, but the intercalated particle dispersion improved the stiffness properties of PET/glass fibers/nanoclay composites.

Keywords: fibre reinforced polymers; nanocomposites; processing; morphology; mechanical properties
PACS: 8105Qk, 82.35 Np, 82.35 Lr

INTRODUCTION

Obtaining controlled morphology of nanoparticles in polymer matrices is the foremost challenge in achieving the advances promised by polymer nanocomposites. Nanoparticles are presently considered to be high-potential filler materials for the improvement of mechanical properties of polymers [1]. Polymer layered silicate nanocomposites have been mostly investigated and used in many industrial applications because of their natural abundance and low cost. Among clay nanoparticles, the most commonly used layered silicate is montmorillonite (MMT), an aluminosilicate smectite clay. MMT is a cation-poor layered silicate that can be easily separated and/or delaminated (exfoliated) [2- 11].

Poly(ethylene terephthalate), PET, is a commodity polymer due to the combination of its low-cost and high performance [2, 3, 12-14]. As a result, it has found applications in many fields: food and beverage packing, luggage, furnishings, appliances and automotive industry. In the latter fields where stiffness is of crucial importance, PET is often reinforced with short glass fibers [14-16]. Nevertheless, the incorporation of glass fibers in polymer matrices leads to processing difficulties, such as increase of viscosity and faster wear of processing equipment.

To answer the industry needs to lighten materials while conserving mechanical properties, the incorporation of nanoparticles in polymer matrices appears as a promising option [2-11, 17-25]. In this case, a low percentage of

nanofillers are desired to both reduce weight and processing equipment wear without compromising the polymer properties and cost.

A chosen route to prepare PET layered silicate nanocomposites is by melt blending techniques [2, 3, 5, 8, 11, 13, 20, 21, 23, 26] due to its environmentally friendly and low cost processing way. The melt intercalation method is remarkable because it can produce both intercalated and exfoliated composites with a wide range of polymers [12]. Materials with adequate performance require that the polymer molecules are intercalated in the clay galleries to promote exfoliation/intercalation, the size of clay agglomerates is substantially reduced and a high dispersion of the particles in the polymer matrix is obtained [7, 8, 11, 13, 22, 24]. The success of the exfoliation is associated with the presence of strong interactions between the clay and the polymer chain [11], in addition to enough mechanical loading and appropriate residence time [3, 22].

In this research work we are interested in studying the influence of nanoclay loadings on the mechanical and morphological properties of glass fiber reinforced PET systems. Industrial processing methods such as extrusion and injection moulding were used for the preparation of PET/glass fiber/MMT composites. The morphology of ternary composites was thoroughly characterized by DSC, DMA, FTIR, XRD and TEM. Mechanical properties were evaluated by tensile tests in order to measure the stress at yield (σ_y) and the Young's modulus (E).

EXPERIMENTAL

Materials

Polymer matrices were supplied by DSM Engineering Plastics: unreinforced PET (Arnite D04 300) has a density of 1.34 g/cm^3 and melting point (10 ºC/min) of 255 ºC; 20 % glass fiber reinforced PET (Arnite AV2 340) has a density of 1.52 g/cm^3 and melting point (10 ºC/min) of 255 ºC. The organically modified montmorillonite is Cloisite 15A supplied by SCP Rockwood Additives. It is treated with a quaternary ammonium salt; it has a density of 1.66 g/cm^3 and ionic interchange capacity of 125 meq/100g.

Processing

The ARNITE D04 300 (neat PET) and the Cloisite15A were dried at 120 ºC for at least 6 h before compounding by extrusion. The blend was processed in a co-rotating twin-screw extruder using two material feeders, a barrel temperature profile from 270 ºC at the feeder to 265 ºC at the die and a screw speed of 100 rpm. At the die exit the masterbatch was immediately cooled down with water and afterwards milled in conventional milling equipment, in small cylinders with 1.3 mm of diameter and 3.0 mm of length.

The PET/MMT masterbatch was added to the pure PET or glass fiber reinforced PET. The pellets were dried at 120 ºC for at least 6 hours after mechanical blending in a tumbler mixer for 30 min.

Dog-bone shaped specimens were molded by injection process, using a Ferromatik-Milacron K85 machine. The injection conditions have been fixed according to the material data sheet, which sum up is in Table 1.

TABLE 1. Injection process conditions according to the technical recommendations.

Material	T_{inj} (ºC)	T_w (ºC)	P_h (bar)	P_b (bar)	V_{inj} (mm.s^{-1})
Pure PET and its nanocomposites	280	23 ± 2	20	5	30
Glass fibre reinforced PET and its nanocomposites	290	130 ± 2	20	5	30

Throughout the paper, the numbers following the designation PET and NC in sample names, indicate the weight percentage of each constituent in the sample. For instance, PET00 designates a sample of pure PET, while PET20NC1.0 designates a sample containing 20 wt% of glass fibers and 1.0 wt% of MMT nanoclay.

Characterization Methods

X-ray diffraction (XRD) was performed in a BRUKER D8 Discover diffractometer. Samples were scanned using a θ/2θ mode of Cu Kα radiation (λ = 1.5406 Å) at a step size of 0.04 °/min and 2θ range from 2º to 10º,

corresponding to a lattice spacing range between 44.14-8.84 Å The interlayer spacing of the nanoclay was determined using the Bragg's law: $\lambda=2d \sin\theta$.

To perform Transmission electron microscopy (TEM), all samples were ultramicrotomed with a diamond knife of Diatome on a Leica EM UC7 microtome at room temperature to give sections with a nominal thickness of 70 nm. The sections were transferred from water (room temperature) to carbon-coated 150-mesh Cu grids. Bright-field images were obtained at 200 kV, under low-dose conditions, with a FEI TECNAI T20 electron microscope.

DSC experiments were performed with a Perkin-Elmer DSC7 in standard mode. Heating scans were performed at a heating rate of 10 ºC/min. Glass transition temperature (Tg), cold crystallization (Tcc) and melting temperature (Tm) were obtained. The calculation of the crystallinity rate (χ_c) is based on a two-phase (crystalline–amorphous) peak area method reported elsewhere [26], considering the melting Hm and the cold crystallization Hcc enthalpies as the areas of the melting peak and crystallization peak, respectively, with the enthalpy of fusion of 100 % crystalline PET, taken to be equal to 120 J/g. The reported results are the average of 3 samples.

Fourier transformed infrared spectrometry (FTIR) was performed with a Perkin Elmer Spectrum One spectrometer equipped with a single refection ATR accessory. All spectra were normalized to equal intensity of the band at 1409 cm^{-1} related to bonds of the aromatic ring, which is insensitive to crystallinity changes.

Dynamic mechanical analysis (DMA) curves were determined from dog bone shaped specimens by using a Rheometrics ARES operating in the torsion mode, at a heating rate of 5.0°C/min and 1.0 rad/s angular frequency. A deformation of 1% within the elastic linear domain was applied to the specimens.

Tensile mechanical behavior of the materials was assessed using a universal testing machine Shimatzu 50 KN. The tests were carried out at room temperature (23 ± 1 ºC), at a strain rate of 1 mm/min. Test specimens were obtained according to standard ISO 527-2: 1993 (E). The tensile modulus (E) and the stress at yield (σ_y) are resulting from the stress-strain curves.

RESULTS AND DISCUSSION

Figure 1 shows the diffraction patterns of Cloisite 15A and masterbatch PET00NC10. Neat Cloisite C15A presents a basal gallery distance of 31.5 Å (2θ = 2.80º). For the masterbatch prepared by extrusion, a sharper and intense peak appears corresponding to approximately d001 = 35.6 Å (2θ = 2.48º). The increasing of 4.1 Å in the interlayer spacing suggests that some PET chains are intercalated into clay gallery space. However, it is difficult to determine whether the C15A is fully intercalated since a large portion of the clay remains as immiscible aggregates.

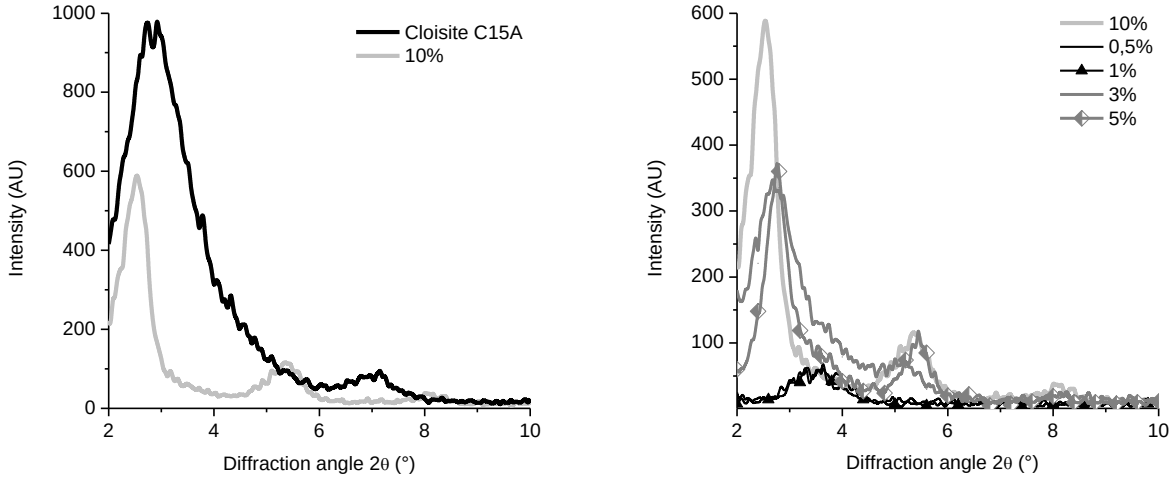

FIGURE 1. XRD patterns - Left: Cloisite15A nanoclay and PET00NC10
Right: PET00NC10 and injection molded samples PET20NC0.5, PET20NC1.0, PET20NC3.0 and PET20NC5.0

PET20NC0.5 and PET20CN1.0 present the broadest peaks and the highest angles, as seen in Fig.1, meaning the lowest gallery distance: d001 = 25.1 Å (2θ = 3.52º) and d001 = 25.4 Å (2θ = 3.48º), respectively, among all mixtures prepared by injection molding. PET20NC3.0 and PET20NC5.0 show the sharpest peaks at the lowest angles, corresponding to d001 = 32.5 Å (2θ = 2.72º) and d001 = 32.0 Å (2θ = 2.76º), respectively. The interlayer spacing of

PET20NC3.0 and PET20NC5.0 is still far from the one of the masterbatch but still higher than the neat nanoclay. As the clay amount is very small and extensively disordered, TEM images were recorded to complement XRD analysis.

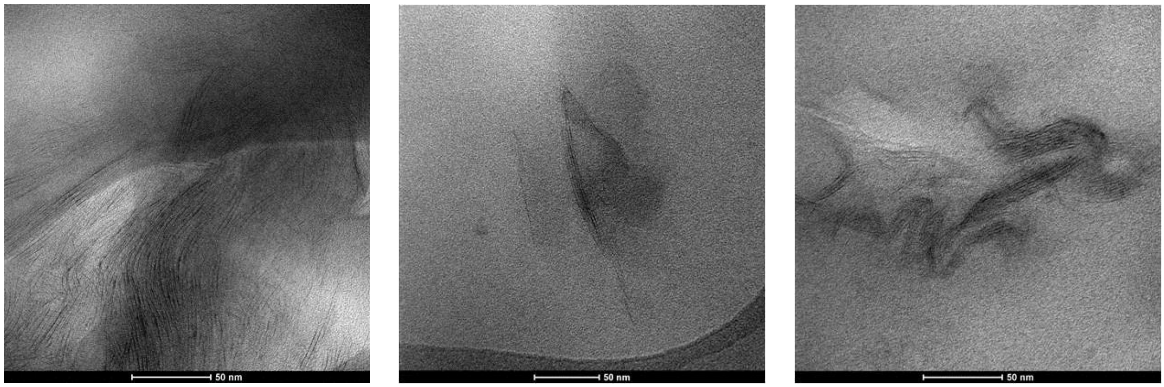

(a) (b) (c)

FIGURE 2. TEM micrographs at the magnification x400000: (a) PET00NC10; (b) PET20NC0.5; (c): PET20NC1.0.

Even with the shear rate involved in the extrusion process, clay platelets are intercalated rather than exfoliated in the masterbatch, as seen in Fig.2a. Samples PET20NC0.5 and PET20NC1.0 containing small amounts of nanoclay show aggregated platelets in Fig.2a and 2b. Both XRD patterns and TEM images reveal that some clay tactoids remain in all nano- and multiscale composites. Exfoliated structure is presumed to be required to impart the nanocomposites with enhanced mechanical properties. However, Bousmina [22] found out that the best enhancement in Young's modulus is exhibited by samples with intermediate level of exfoliation, meaning a percolation network, rather than fully exfoliated.

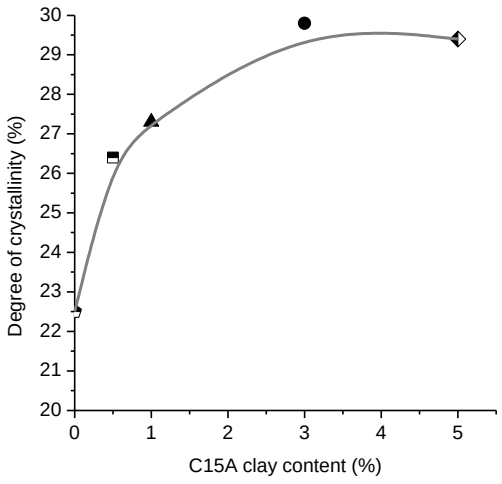

FIGURE 3. Crystalline rate as a function of clay content for ternary composites

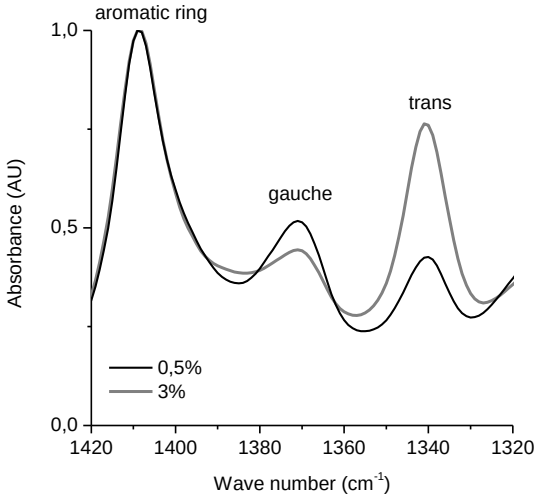

FIGURE 4. Normalized IR spectra of the samples PET20NC0.5 and PET20NC3.0.

Figure 3 shows the variation of crystallinity measured from DSC experiments for glass fiber reinforced PET with various amounts of C15A. The crystalline rate increases with Cloisite15A fraction and the highest value was found for 3.0 wt% of nanoclay. This can be explained by rapid crystallization due to the nucleating effect of the fillers [8, 25]. Another possible reason is that MMT nano-structure itself can help the PET molecules stack on each other to grow into crystallites [23]. This result is confirmed by FTIR experiment as seen in Fig.4, in which we show the change in crystallinity by monitoring the band at 1340 cm^{-1}, which is attributed to the trans conformation of the H_2C-CH_2 bond, hence the crystalline phase, and the band at 1370 cm^{-1} for the gauche conformation, representative of the amorphous phase.

Elastic G' and viscous G" responses obtained from dynamic mechanical analysis are presented respectively in Fig.5 and Fig.6 as a function of temperature. The addition of nanoclay into the polymer system has no effect on the elastic modulus in the glassy state. From 60°C, the curves slope harshly down, marking out the transition from the

glassy state to the rubbery state, Tg. It is found in Fig. 6 that the peak representing Tg broadens as nanoclay content increases. Clay nanoparticles create domains with various relaxation times. Indeed, as C15A content increases, the clay/polymer interfaces ratio increases and, more polymer chains are trapped between clay platelets as revealed by XRD; the latter move with different relaxation times compared to the bulk.

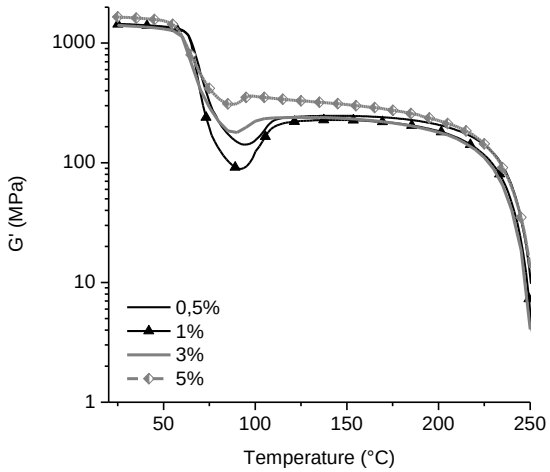

FIGURE 5. Elastic modulus response G' of the material upon temperature changes.

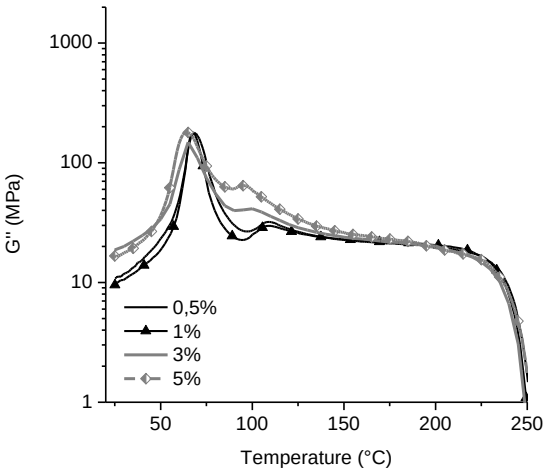

FIGURE 6. Loss modulus response G" of the material upon temperature changes.

Right beyond Tg, the polymer chains are enough mobile to self-organize in the step called cold crystallization, as seen on both elastic and viscous curves. The wide temperature range as well as the large amplitude observed for the samples with 0.5% and 1% of nanoclay in Fig.6, reveals the crystallization takes place uneasily in these samples compared to 3 and 5% of nanoclay. After 230°C, both elastic and viscous moduli fall drastically, pointing out the melting of PET.

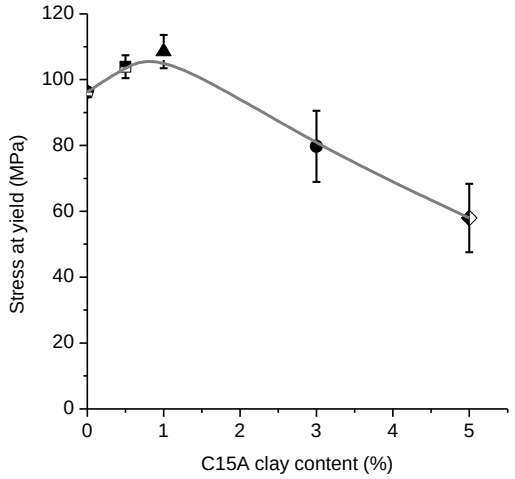

FIGURE 6. Stress at yield results of ternary composites as a function of C15A content.

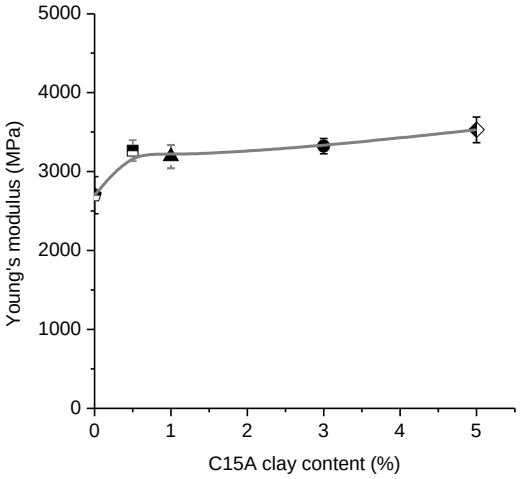

FIGURE 7. Young's modulus results of ternary composites as a function of C15A content.

Figure 6 shows stress at yield versus Cloisite C15A contents. An increase of the yield stress is only observed for additions of C15A up to 1 wt%. For nanoclay contents of 3 and 5 wt%, the yield stress shows a reduction of about 17 and 19 %, respectively as compared to pure PET. This trend is in accordance with other works [23]. Jordan and al. [18] found out that, for systems with good particle-polymer interaction, the yield stress tends to increase with increasing filler volume fraction. The opposite is revealed for poor interaction systems. Fig. 7 shows that Young's modulus increases with an increment of the C15A content. Whereas the increase is significant when the C15A content varies from 0 to 0.5%, this increase is lower for other concentrations. For 5 wt% of nanoclay content, the Young's modulus is increased by 35% compared to PET20. The Young's modulus of a polymeric material has been shown to be remarkably improved when nanocomposites are formed [9,18].

CONCLUSION

Multiscale PET/glass fibers/nanoclay composites were prepared using industrial processes such as extrusion and injection moulding. Their morphology, structure and mechanical properties were studied.

XRD and TEM revealed that the nanoclay presents an intercalated morphology rather than exfoliated in all investigated samples. The extrusion process enlarges the interlayer distance from 31.5 Å for the neat clay to 35.6 Å for the PET00NC10. As unexpected, the interlayer distance is narrower for subsequently injection-molded specimens. Indeed, the interlayer distance decreases to 32.0 Å. Thus, these results indicate that melt blending can produce intercalating type of PET/organo-MMT nanocomposite. Even though some polymer chains are intercalated into nanoclay layers due to extrusion conditions, the unfavorable interactions between polymer and nanoclay leads the platelets to re-aggregate during the injection step, because of high pressure. The addition of C15A increases the degree of crystallinity, as shown by DSC and FTIR, suggesting that MMT acts as a nucleating agent. The distribution of relaxation times broadens as nanoclay content increases, as revealed by DMA, indicating a change in molecular mobility at clay/polymer interfaces. The tensile strength of composites with 0.5 and 1 wt% of C15A is enhanced. It seems that the multiscale composites have an optimum comprehensive mechanical property when the C15A content is equal to 1 wt%. For more than 3% of nanoclay, the tensile strength decreases, in accordance with other works [23].

Indeed, clay exfoliation was not attained, but the intercalated particle dispersion improved the stiffness properties of PET/glass fibers/nanoclay composites, as revealed by the increase of Young's modulus values.

ACKNOWLEDGMENTS

The authors would like to thank Southern Clay Products and DSM for donation of nanoclays and PET materials, respectively. This work was supported by TECNA: INTERREG IV-B SOE1/P1/E184. We would also like to thank N. Garcia and L. Figueras from INA-UZ (Instituto de Nanociencia de Aragón da Universidad de Zaragoza), and A. Moubarik (Ecole Nationale d'Ingénieurs de Tarbes) for DMA experiments.

REFERENCES

1. J. Njuguna, K. Pielichowski, S. Desai. Polymers for Advanced Technologies 2008; 19: 947-959.
2. X.Xu, Y.Ding, Z. Qian, F. Wang, B. Wen, H. Zhou, S. Zhang, M. Yang. Pol. Degrad. and Stability 2009; 94: 113-123.
3. C. I. W. Calcagno, C. M. Marini, S. R. Teixeira, R. S. Mauler. Polymer 2007; 48: 966-974.
4. A. B. Morgan, J. W. Gilman. J. of Applied Pol. Sci., 2003; 87: 1329-1338.
5. I. F. Leite, C. M. O. Raposo, L. H. Carvalho, S. M. L. Silva. Revista Matéria, 2006; 11: 260-266.
6. M. Herman F. Encyclopedia of Polymer Science and Technology. New Jersey: John Wiley & Sons; 2003.
7. M. Le Bras, S. Bourbigot, S. Duquesne, C. Jama, C. Wilkie, Cambridge: The Royal Society Chemistry; 2005.
8. A. Sanchez-Solís, I. Romero-Ibarra, M. R. Estrada, F. Calderas, O. Manero. Pol. Eng. and Sci. 2004; 44: 1094-1102.
9. S. S. Ray, M. Okamoto. Progress in Polymer Science 2003; 28: 1539–1641.
10. M. Alexander, P. Dubois. Materials Science and Engineering 2000; 28: 1-63.
11. A. Sanchez-Solís, A. Garcia-Rejon, M. Estrada, A. Martinez-Richa, G. Sanchez, O. Manero. Pol. Intern. 2005; 54: 1669-1672.
12. M.-C. Lai, K.-C. Chang, W.-C. Huang, S.-C. Hsu, J.-M. Yeh. J. of Physics and Chemistry of Solids 2008; 69: 1371-1374.
13. C. H. Davis, L. J. Mathias, J. W. Gilman, D. A. Schiraldi, J. R. Shields, et al. J. of Pol. Sci. Part B, 2002; 2661-2666.
14. A. Pegoretti, J. Kolarik, M. Slouf. eXPRESS Polymer Letters 2009; 3: 235-244.
15. I. Rezaeian, S. H. Jafari, P. Zahedi, S. Nouri. Polymer Composites 2009; 993-999.
16. M. Krácalík, L. Pospísil, M. Slouf, J. Mikesová, A. Sikora, J. Simoník, I. Fortelný. Pol. Composites, 2008 ; 29: 915–921.
17. R. S. Rajeev, E. Harkin-Jones, K. Soon, T. McNally, G. Menary, C. G. Armstrong, P. J. Martin. Europ. Pol. J. 2009; 45: 332-340.
18. J. Jordan, K. I. Jacob, R. Tannenbaum, M.A. Sharaf, I. Jasiuk. Materials Sci. and Eng. 2005; 393: 1-11.
19. J. W. Gilman S. Bourbigot, J. R. Shields, M. Nyden, T. Kashiwagi, R. D. Davis, et al.,. J. of Materials Sci. 2003; 38: 4451-4460.
20. G. D. Barber, B. H. Calhoun, R. B. Moore. Polymer 2005; 46: 6706-6714.
21. A. Sanchez-Solís, A. Garcia-Rejon, O. Manero. Macromol. Symp. 2003; 192: 281-292.
22. Bousmina, Mosto. Macromolecules 2006; 39: 4259-4263.
23. Y. Wang, J. Gao, Y. Ma, U. S. Agarwal. Composites Part B: engineering 2006; 37: 399-407.
24. D. W. Litchfield, D. G. Baird. Polymer 2008; 49: 5027-5036.
25. B. G. Girija, R. R. N. Sailaja, G. Madras. Polymer Degradation and Stability 2005; 90: 147-153.
26. L. V. Todorov, J. C. Viana, Journal of Applied Polymer Science 2007; 1659-1669.
27. L. V. Todorov, C. I. Martins, J. C. Viana, Solid State Phenomena 2009; 151: 113-117.